

Electronic states bound by repulsive potentials in graphene irradiated by a circularly polarized electromagnetic field

O. V. Kibis^{1,*}, M. V. Boev¹, I. V. Iorsh^{1,2}, and V. M. Kovalev¹

¹*Department of Applied and Theoretical Physics, Novosibirsk State Technical University, Karl Marx Avenue 20, Novosibirsk 630073, Russia and*

²*Department of Physics, Queen's University, Kingston, Canada*

In the framework of the Floquet theory of periodically driven quantum systems, it is demonstrated that irradiation of graphene by a circularly polarized electromagnetic field induces an attractive area in the core of repulsive potentials. Consequently, the quasi-stationary electron states bound by the repulsive potentials appear. The difference between such field-induced states in graphene and usual systems with the parabolic dispersion of electrons is discussed and possible manifestations of these states in electronic transport and optical spectra of graphene are considered.

I. INTRODUCTION

The control of conduction electrons in condensed-matter structures by a high-frequency off-resonant electromagnetic field — also known as the Floquet engineering — has become an excited area of modern physics^{1–10}. If a field frequency much exceeds characteristic electron frequencies, the field cannot be absorbed by electrons but only dresses them. As a result, such a dressing field substantially modifies electronic properties of various nanostructures, including quantum rings^{11,12}, quantum wells¹³, topological insulators^{14–17}, Moiré structures^{18–20}, materials with tilted Dirac cones^{21–23}, graphene^{24–31} and related two-dimensional materials^{32–34}, etc. Particularly, it was found recently that a circularly polarized electromagnetic field can induce an attractive area in the core of two-dimensional (2D) repulsive potentials³⁵. This results in the quasi-stationary electron states bound by the repulsive potentials, which substantially modify electronic properties of irradiated 2D systems^{36–38}. However, the theory of these states was developed before only for 2D systems with the parabolic dispersion of electrons. The present article is aimed to extend the theory over 2D systems with the linear (Dirac) electron dispersion which takes place in graphene and related materials.

The article is organized as follows. In Sec. II, the model of the discussed effect is developed. In Sec. III, possible manifestations of the optically induced quasi-stationary electron states bound by repulsive potentials in transport and optical phenomena are discussed. The last two sections contain the conclusion and acknowledgements.

II. MODEL

Let us consider a graphene sheet which lies in the plane (x, y) and is subjected to a circularly polarized electromagnetic wave propagating perpendicularly to the plane (see Fig. 1a). Then electronic properties of the irradiated graphene sheet near its Dirac point are described by the

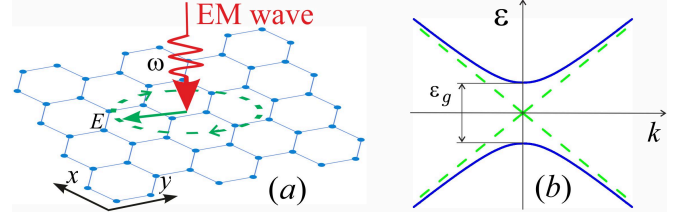


FIG. 1: (a) Sketch of the system under consideration: Graphene irradiated by a circularly polarized electromagnetic wave with the frequency ω and the electric field amplitude E ; (b) Energy band structure of graphene near the Dirac point in the presence of circularly polarized irradiation (solid lines) and in the absence of one (dashed lines).

Hamiltonian^{25,26}

$$\hat{\mathcal{H}} = v_0 \boldsymbol{\sigma} \cdot (\hbar \mathbf{k} - e \mathbf{A}(t)/c), \quad (1)$$

where $\boldsymbol{\sigma} = (\sigma_x, \sigma_y)$ is the Pauli matrix vector, $\mathbf{k} = (k_x, k_y)$ is the electron wave vector in the graphene plane, v_0 is the electron velocity in graphene near the Dirac point ($\mathbf{k} = 0$), e is the electron (hole) charge,

$$\mathbf{A}(t) = (A_x, A_y) = \frac{cE}{\omega} (\cos \omega t, \sin \omega t) \quad (2)$$

is the vector potential of the electromagnetic wave, E is the electric field amplitude of the wave, and ω is the wave frequency. Solving the Schrödinger problem with the periodically time-dependent Hamiltonian (1), it was demonstrated earlier that the circularly polarized field (2) opens the band gap in the Dirac point^{25,26},

$$\epsilon_g = \sqrt{(\hbar\omega)^2 + 4W^2} - \hbar\omega, \quad (3)$$

where $W = v_0|e|E/\omega$ is the kinetic energy of electron (hole) rotation under the field (see Fig. 1b). In the following, we will assume that the field (2) is strong enough to satisfy the condition

$$W \gg \hbar\omega. \quad (4)$$

Under this condition, the interband absorption of the field (2) is forbidden by the energy conservation law since

the band gap (3) much exceeds the photon energy. To proceed, let us rewrite the Hamiltonian (1) in the matrix form as

$$\hat{\mathcal{H}} = \hbar v_0 \begin{pmatrix} 0 & k_x - ik_y \\ k_x + ik_y & 0 \end{pmatrix} - \frac{v_0 e}{c} \begin{pmatrix} 0 & A_x - iA_y \\ A_x + iA_y & 0 \end{pmatrix} = \begin{pmatrix} 0 & \varepsilon_{\mathbf{k}} e^{-i\theta} \\ \varepsilon_{\mathbf{k}} e^{i\theta} & 0 \end{pmatrix} \quad (5)$$

and apply the unitary transformation

$$\hat{U} = \frac{1}{\sqrt{2}} \begin{pmatrix} e^{-i\theta/2} & e^{-i\theta/2} \\ e^{i\theta/2} & -e^{i\theta/2} \end{pmatrix}, \quad (6)$$

where

$$\theta = \arctan \left(\frac{\hbar k_y - (eE/\omega) \sin \omega t}{\hbar k_x - (eE/\omega) \cos \omega t} \right), \quad (7)$$

and

$$\varepsilon_{\mathbf{k}} = v_0 \sqrt{(\hbar k_x - eA_x/c)^2 + (\hbar k_y - eA_y/c)^2}. \quad (8)$$

Then the unitary transformed Hamiltonian (5) reads

$$\hat{\mathcal{H}}' = \hat{U}^\dagger \hat{\mathcal{H}} \hat{U} - i\hbar \hat{U}^\dagger \partial_t \hat{U} = \begin{pmatrix} \varepsilon_{\mathbf{k}} & f_{\mathbf{k}} \\ f_{\mathbf{k}} & -\varepsilon_{\mathbf{k}} \end{pmatrix}, \quad (9)$$

where

$$f_{\mathbf{k}} = \frac{\hbar \omega}{2} \left[\frac{(\hbar v_0^2 e/c) \mathbf{k} \cdot \mathbf{A}(t) - W^2}{\varepsilon_{\mathbf{k}}^2} \right]. \quad (10)$$

It follows from Eq. (8) that the diagonal terms of the Hamiltonian (9) are identical to the electron energy spectrum of graphene, $\varepsilon(\mathbf{k}) = \pm \hbar v_0 \sqrt{k_x^2 + k_y^2}$, with the replacement $\hbar k_{x,y} \rightarrow \hbar k_{x,y} - eA_{x,y}/c$. Physically, they describe the time evolution of electron (hole) states within the conduction (valence) band of graphene under the field (2). As to the non-diagonal terms (10), they describe the mixing of the conduction and valence bands by the field. Under the condition (4), these non-diagonal terms contribute to the electron states near the band edges with the smallness $\sim \hbar \omega / W$ and, therefore, can be omitted as a first approximation. Then the diagonal terms of the Hamiltonian (9) yield the electron dispersion near the band edge ($\hbar v_0 k \ll W$),

$$\varepsilon_{\pm}(\mathbf{k}) \approx \pm W \mp \frac{e}{|e|} \hbar v_0 (k_x \cos \omega t + k_y \sin \omega t) \pm \frac{\hbar^2 v_0^2}{2W} (k_x^2 \sin^2 \omega t + k_y^2 \cos^2 \omega t - k_x k_y \sin 2\omega t), \quad (11)$$

where the signs “+” and “−” correspond to the conduction and valence band, respectively. Replacing the momentum $\hbar \mathbf{k} = (\hbar k_x, \hbar k_y)$ in Eq. (11) with the momentum operator $\hat{\mathbf{p}} = (\hat{p}_x, \hat{p}_y)$, we arrive at the Hamiltonian

$$\hat{\mathcal{H}}_{\pm} = \pm W \mp \frac{e}{|e|} v_0 (\hat{p}_x \cos \omega t + \hat{p}_y \sin \omega t) \pm \frac{v_0^2}{2W} (\hat{p}_x^2 \sin^2 \omega t + \hat{p}_y^2 \cos^2 \omega t - \hat{p}_x \hat{p}_y \sin 2\omega t), \quad (12)$$

which describes the dynamics of charge carriers in the scatterer potential $U(\mathbf{r})$ near the band edge.

To remove the linear terms $\propto \hat{p}_{x,y}$ from the Hamiltonian (12), let us apply the Kramers-Henneberger (KH) unitary transformation^{39,40}. In the considered case of irradiated graphene, the KH transformation operator is

$$\hat{U}_{\pm} = \exp \left\{ \pm \frac{i}{\hbar} \int^t \left[v_0 \frac{e \mathbf{A}(\tau)}{|e \mathbf{A}(\tau)|} \hat{\mathbf{p}} - W \right] d\tau \right\} \quad (13)$$

and, correspondingly, the unitary transformed Hamiltonian (12) reads

$$\hat{\mathcal{H}}'_{\pm} = \hat{U}_{\pm}^\dagger \hat{\mathcal{H}}_{\pm} \hat{U}_{\pm} - i\hbar \hat{U}_{\pm}^\dagger \partial_t \hat{U}_{\pm} = U(\mathbf{r} - \mathbf{r}_0(t)) \pm \frac{v_0^2}{2W} (\hat{p}_x^2 \sin^2 \omega t + \hat{p}_y^2 \cos^2 \omega t - \hat{p}_x \hat{p}_y \sin 2\omega t), \quad (14)$$

where

$$\mathbf{r}_0(t) = r_0^* (-\sin \omega t, \cos \omega t) \quad (15)$$

is the radius vector of circular trajectory of a charge carrier in graphene under the field (2), and

$$r_0^* = \frac{v_0}{\omega} \quad (16)$$

is the radius of the trajectory. It should be noted that the Hamiltonian (14) with the periodically time-dependent potential is still physically identical to the Hamiltonian (12). Next, we need to make the high-frequency approximation. It follows from the conventional Floquet theory of periodically driven quantum systems that one can introduce the unitary transformation, $\hat{U}_0(t)$, turning the time-dependent Hamiltonian (14) into the effective stationary Hamiltonian,

$$\hat{\mathcal{H}}_{\text{eff}} = \hat{U}_0(t)^\dagger \hat{\mathcal{H}}'_{\pm} \hat{U}_0(t) - i\hbar \hat{U}_0^\dagger(t) \partial_t \hat{U}_0(t), \quad (17)$$

which can be written as an expansion in powers of $1/\omega$ (the Floquet-Magnus expansion)³⁻⁶,

$$\hat{\mathcal{H}}_{\text{eff}} = \hat{\mathcal{H}}_0 + \sum_{n=1}^{\infty} \frac{[\hat{\mathcal{H}}_n, \hat{\mathcal{H}}_{-n}]}{n\hbar\omega} + O\left(\frac{1}{\omega^2}\right), \quad (18)$$

where $\hat{\mathcal{H}}_n$ are the Fourier harmonics of the time-dependent Hamiltonian (14), $\hat{\mathcal{H}}'_{\pm} = \sum_{n=-\infty}^{\infty} \hat{\mathcal{H}}_n e^{in\omega t}$. In the high-frequency limit, one can restrict the expansion (18) by its main term,

$$\hat{\mathcal{H}}_0 = \pm \frac{\hat{\mathbf{p}}^2}{2m_e^*} + U_0(\mathbf{r}), \quad (19)$$

where

$$m_e^* = \frac{2|e|E}{v_0\omega} \quad (20)$$

is the field-induced effective mass of charge carriers in the irradiated graphene, and the time-averaged potential

$$U_0(\mathbf{r}) = \frac{1}{2\pi} \int_{-\pi}^{\pi} U(\mathbf{r} - \mathbf{r}_0(t)) d(\omega t) \quad (21)$$

can be treated as a repulsive potential $U(\mathbf{r})$ dressed by the circularly polarized field (2). In the following, the effective stationary Hamiltonian (19) will be applied to describe electron dynamics in this potential.

III. RESULTS AND DISCUSSION

The Hamiltonian (19) is equal to the Hamiltonian describing an irradiated 2D system with the parabolic electron dispersion if to make the replacements $m_e^* \rightarrow m_e$ and $r_0^* \rightarrow r_0$, where m_e is the effective electron mass corresponding to the parabolic electron energy spectrum $\varepsilon(\mathbf{k}) = \hbar^2 \mathbf{k}^2 / 2m_e$ and $r_0 = |e|E / m_e \omega^2$ is the radius of circular trajectory of an electron in the 2D system under the field (2) (see Ref. 36). Therefore, the behavior of electrons describing by these Hamiltonians is qualitatively similar. Particularly, it was demonstrated earlier that the dressed potential (21) originated from an repulsive potential of most general form acquires the local minimum in its core, which leads to electron states confined near this minimum³⁵. Restricting the analysis by the case of short-range scatterers and modelling their repulsive potential by the delta function, $U(\mathbf{r}) = u_0 \delta(\mathbf{r})$, the dressed potential (21) reads³⁶

$$U_0(\mathbf{r}) = \frac{u_0 \delta(r - r_0^*)}{2\pi r_0^*}, \quad (22)$$

where $u_0 > 0$ signifies the strength of the repulsive potential, and $\mathbf{r} = (x, y)$ is the plane radius vector. Consequently, the dressing field given by Eq. (2) transforms the repulsive delta potential into a ring-shaped delta potential barrier described by Eq. (22). This transformation leads to the confinement of electron states within the enclosed region $0 < r < r_0^*$. Since the radius (16) is the localization scale of these electron states, they satisfy the long-wavelengths regime if the radius r_0^* much exceeds the lattice constant a_0 . Thus, the developed theory is applicable to short-range repulsive potentials under the condition $r_0^* \gg a_0$. It should be noted that the discussed bound states are quasi-stationary because they can decay by tunneling through the potential barrier into the continuum of free electron states, as it is pictured in Fig. 2a. As a result, these states acquire energy broadening. If the repulsive potential is strong enough ($\alpha = 2\hbar^2/m_e^* u_0 \ll 1$), the previously derived expressions can be applied to describe electron states bound by repulsive potentials in irradiated 2D systems with parabolic electron dispersion (see Ref. 36). Namely, the replacements $m_e \rightarrow m_e^*$ and $r_0 \rightarrow r_0^*$ in these expressions yield the energy spectrum of the bound states in irradiated graphene,

$$\varepsilon_{nm} = \frac{\hbar^2 \omega^3 \xi_{nm}^2}{4|e|E v_0} + O(\alpha), \quad (23)$$

their energy broadening

$$\Gamma_{nm} = \frac{4\varepsilon_{nm}\alpha^2}{|N_m^3(\xi_{nm})[J_{|m|+1}(\xi_{nm}) - J_{|m|-1}(\xi_{nm})]|} + O(\alpha^3), \quad (24)$$

and their wave functions

$$\psi_{nm} = \frac{e^{im\varphi}\omega}{\sqrt{\pi}v_0 J_{|m|+1}(\xi_{nm})} \begin{cases} J_m\left(\frac{\xi_{nm}\omega r}{v_0}\right), & 0 < r \leq r_0^* \\ 0, & r \geq r_0^* \end{cases} + O(\alpha), \quad (25)$$

where $J_m(\xi)$ and $N_m(\xi)$ are the Bessel functions of the first and second kind, respectively, ξ_{nm} is the n th zero of the Bessel function $J_m(\xi)$ (i.e. $J_m(\xi_{nm}) = 0$), $n = 1, 2, 3, \dots$ is the quantum number enumerating zeros of the Bessel function $J_m(\xi)$, and $m = 0, \pm 1, \pm 2, \dots$ is the angular momentum. The dependence of the ground state energy ε_{10} on the field frequency ω and the field amplitude E is plotted in Fig. 2b. Although the structure of the bound states in electronic systems with the linear and parabolic dispersions is qualitatively similar, the dependence of the states on the field in these systems is substantially different. First, it should be stressed that the bound states exist if the radius of circular trajectory of an electron under the field (2) much exceeds the crystal lattice spacing, a_0 . In 2D systems with the parabolic electron dispersion³⁶, this radius is $r_0 = |e|E / m_e \omega^2$ and, therefore, the condition $r_0 \gg a_0$ can be satisfied in the considered high-frequency limit only for extremely strong field amplitudes E . Since such a strong field can destroy a 2D sample, observation of the bound states in 2D systems with the parabolic electron dispersion is experimentally difficult. In graphene, this radius r_0^* is defined by Eq. (16) and does not depend on the field amplitude E . As a consequence, the condition $r_0^* \gg a_0$ can be satisfied for any field amplitude in the broad frequency range due to the giant electron velocity v_0 . Second, it should be noted that the bound state energy in graphene (23) is $\varepsilon_{nm} \propto 1/E$, whereas this energy in usual 2D systems with the parabolic electron dispersion³⁶ is $\varepsilon_{nm} \propto 1/E^2$. Therefore, the bound state energy in graphene under the condition (4) much exceeds this energy in usual 2D systems. As a consequence, observation of the considered bound states in graphene is most convenient from experimental viewpoint. It follows from Eqs. (23)–(25), particularly, that the repulsive potentials confining electron states under a high-frequency field can be considered as quantum dots of new kind if the energy broadening of these states (24) is small enough. In the following, let us discuss possible manifestations of the bound states in electronic transport and optical properties of irradiated graphene.

The resistivity of graphene per area, ρ , arising from the scattering of conduction electrons through the quasi-stationary bound state with the energy ε_{nm} (the Breit-Wigner resonant scattering) is defined at the zero tem-

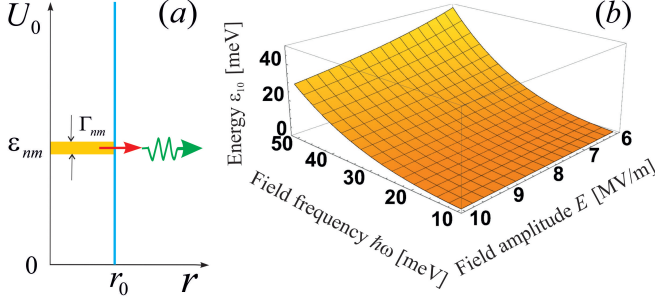


FIG. 2: The energy spectrum of the electron states localized at a repulsive potential: (a) the tunneling of an electron marked by the arrow from the bound state with the energy ε_{nm} and the broadening Γ_{nm} to the state of free conduction electron (the wave arrow) through the delta potential barrier (the vertical line); (b) the dependence of the ground bound state energy ε_{10} on the field frequency ω and the field amplitude E .

perature by the expression³⁶

$$\rho = \frac{2n_0}{\pi n_e} \left(\frac{h}{e^2} \right) \frac{(\Gamma_{nm}/2)^2}{(\varepsilon_F - \varepsilon_{nm})^2 + (\Gamma_{nm}/2)^2}, \quad (26)$$

where h/e^2 is the resistivity quantum, n_0 is the surface density of repulsive scatterers, and ε_F is the Fermi energy. It follows from Eq. (26) that the resistivity depends on the Fermi energy ε_F resonantly. The resonance takes place for $\varepsilon_F = \varepsilon_{nm}$ and the amplitude of this resonance is $\rho_0 = (2n_0/\pi n_e)(h/e^2)$. The dependence of the resistivity (26) on the field frequency ω for the ground bound state ε_{10} is plotted in Fig. 3 for different electron densities. It follows from the plot that the resonant amplitude of the resistivity (26) is large enough to be observed experimentally, $\rho_0 \sim \Omega$, even if the scatterer density is very small, $n_0 \sim 10^{-4}n_e$. In the developed theory, the mean free path of conduction electrons, $\ell \sim n_0^{-1/2}$, is assumed to be large enough, $\ell \gg r_0^*$. If the mean free path ℓ becomes comparable to the radius of the localized electron state r_0^* , the electron states confined by the dressed potential become substantially modified. Namely, due to the tunnelling of electrons between the individual confining potentials, the energies of these states become split. Consequently, an electron may hop between the individual confining potentials, which forms the additional channel of electron transport. It should be noted that the localization length of conduction electrons, ξ , also depends on the radius r_0^* . Indeed, it is described by the known expression $\xi = \sqrt{D\tau_\varphi}$, where $D \sim v\ell$ is the diffusion coefficient of conduction electrons, v is the averaged velocity of electrons, and τ_φ is the coherence time of the electron wave function restricted by inelastic processes. Since r_0^* is the effective radius of an impurity, the increasing of it leads to decreasing the mean free path ℓ and, correspondingly, to decreasing the localization length. However, this effect is weak since the localization length ξ normally much exceeds the radius r_0^* . From viewpoint of possible superconductivity in irradiated 2D systems, it should

be noted that trapping conduction electrons by dressed impurities decreases the density of conduction electrons, which can act on the electron pairing as a destructive factor.

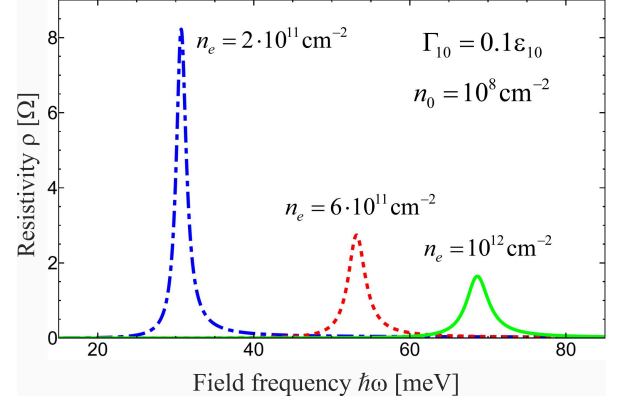


FIG. 3: Dependence of the resistivity per area, ρ , on the field frequency ω for the resonant scattering through the ground bound state ε_{10} with the energy broadening $\Gamma_{10} = 0.1\varepsilon_{10}$, scatterer density $n_0 = 10^8 \text{ cm}^{-2}$ and different electron densities n_e .

The Kondo effect — the minimum of electrical resistivity as a function of temperature — occurs due to the spin interaction between conduction electrons and electrons bound by magnetic impurities^{41–45}. However, the spin interaction between confined electron states (23) and free conduction electrons can lead to the Kondo effect as well. When a localized electron stays in its ground state ε_{10} , this interaction can be effectively described by the Hamiltonian³⁸

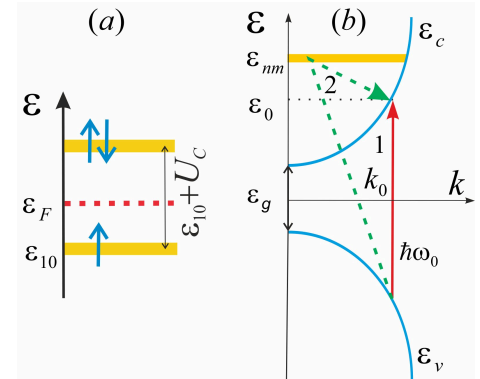


FIG. 4: (a) The singly-occupied (\uparrow) and doubly-occupied ($\uparrow\downarrow$) localized electron state ε_{10} near the Fermi energy ε_F ; (b) Optical transitions from the valence band ε_v to the conduction band ε_c induced by the probing field with the frequency ω_0 : the direct transition (the arrow 1) and the transition through the intermediate bound electron state with the energy ε_{nm} (the arrow 2).

$$\begin{aligned} \hat{\mathcal{H}}_K = & \sum_{\mathbf{k},\sigma} (\varepsilon_{\mathbf{k}} - \varepsilon_F) \hat{c}_{\mathbf{k}\sigma}^\dagger \hat{c}_{\mathbf{k}\sigma} + \sum_{\sigma} (\varepsilon_{10} - \varepsilon_F) \hat{d}_\sigma^\dagger \hat{d}_\sigma \\ & + U_C \hat{d}_\uparrow^\dagger \hat{d}_\uparrow \hat{d}_\downarrow^\dagger \hat{d}_\downarrow + \sum_{\mathbf{k},\sigma} T_{\mathbf{k}} \left[\hat{c}_{\mathbf{k},\sigma}^\dagger \hat{d}_\sigma + \text{H.c.} \right], \quad (27) \end{aligned}$$

where $\varepsilon_{\mathbf{k}} = \hbar^2 k^2 / 2m_e^*$ is the energy spectrum of conduction electrons, the symbol $\sigma = \uparrow, \downarrow$ describes the spin orientation, $\hat{c}_{\mathbf{k},\sigma}^\dagger (\hat{c}_{\mathbf{k},\sigma})$ are the creation (annihilation) operators for delocalized electrons, $\hat{d}_\sigma^\dagger (\hat{d}_\sigma)$ are the creation (annihilation) operators for localized electrons (23),

$$U_C = e^2 \int d^2\mathbf{r} \int d^2\mathbf{r}' \frac{|\psi_{10}(r)|^2 |\psi_{10}(r')|^2}{|\mathbf{r} - \mathbf{r}'|} = \frac{\gamma e^2 \omega}{\epsilon v_0}, \quad (28)$$

is the energy of the Coulomb interaction between two electrons with opposite spin directions $\sigma = \uparrow, \downarrow$ occupying the state (23), ϵ is the permittivity, $\gamma \approx 0.8$ is the numerical constant, and $T_{\mathbf{k}}$ denotes the tunneling matrix element which links the localized electron state (23) with the delocalized electron state characterized by the wave vector \mathbf{k} . From a physical standpoint, the first component of the Hamiltonian (27) represents the energy of delocalized electrons, the second component accounts for the energy of electrons localized in the state (23), the third component describes the Coulomb energy of the doubly occupied state (23), and the fourth component is responsible for the tunneling between the localized and delocalized electron states. When tunneling is sufficiently weak, the localized eigenstates of the Hamiltonian (27) correspond to the singly occupied state (23) with the energy $\varepsilon_{10} - \varepsilon_F$, and the doubly occupied state (23) with the energy $2(\varepsilon_{10} - \varepsilon_F) + U_C$. These states are indicated in Fig. 4a by the symbols \uparrow and $\uparrow\downarrow$, respectively. The Kondo effect emerges due to the spin of a localized electron and can occur when the singly occupied state is filled, while the doubly occupied state remains empty. At the zero temperature, this is represented by the conditions $\varepsilon_{10} - \varepsilon_F < 0$ and $U_C > \varepsilon_F - \varepsilon_{10}$. Consequently, the irradiation-induced Kondo effect in graphene is feasible within the range of field parameters E and ω which meet the inequality

$$\sqrt{\frac{\hbar^2 v_0 \omega \xi_0^2}{4|e|E\varepsilon_F}} < \frac{v_0}{\omega} < \frac{\gamma e^2}{2\epsilon\varepsilon_F} + \sqrt{\frac{\hbar^2 v_0 \omega \xi_0^2}{4|e|E\varepsilon_F} + \left(\frac{\gamma e^2}{2\epsilon\varepsilon_F}\right)^2}. \quad (29)$$

Let us stress that the Hamiltonian (27) is equal to the Anderson Hamiltonian which is fundamental in explaining the microscopic mechanism of magnetic moment formation in metals⁴⁶. Therefore, the established Schrieffer-Wolff (SW) unitary transformation⁴⁷ can be applied to convert the Hamiltonian (27) into the Hamiltonian associated with the Kondo problem⁴⁵, which defines such a characteristic energy scale of the Kondo effect as the Kondo temperature (see Ref. 38 for further details). By substituting $m_e \rightarrow m_e^*$ and $r_0 \rightarrow r_0^*$ into the previously developed Kondo problem theory for an irradiated 2D system with the parabolic electron dispersion³⁸, one can

find that the Kondo temperature in graphene is of several Kelvin for the field (2) with the reasonable parameters $\hbar\omega \sim \text{meV}$ and $E \sim \text{MV/m}$. Thus, the Kondo effect in irradiated graphene can be observable using state-of-the-art experimental techniques.

To detect the bound electron states (23) by optical methods, graphene should be irradiated by an electromagnetic field consisting of the two modes: The first mode is the strong off-resonant field (2) which yields the bound states, whereas the second one is the weak probing resonant field with the amplitude E_0 and the frequency ω_0 , which generates the electron transitions between the valence and conduction bands of graphene. Therefore, both the direct interband electron transitions (marked by the solid arrow 1 in Fig. 4b) and the interband electron transitions through intermediate bound states (marked by the dashed arrow 2 in Fig. 4b) take place. To describe the low-energy optical properties, it is enough to take into account only the ground bound state ε_{10} . Assuming the scatterer density to be small enough, $n_0 r_0^{*2} \ll 1$, the intensity of the probing field absorption, which arises from these two types of optical transitions, is described by the expression³⁷

$$\begin{aligned} I = & \left(\frac{\omega_0 m_e^* |D_{cv}|^2 E_0^2}{2\hbar^2} \right) \left[1 + \frac{\hbar^2 n_0^2 \Gamma_{10} \Phi_{10}^2(k_0)}{m_e^* [(\varepsilon_0 - \varepsilon_{10})^2 + (\Gamma_{10}/2)^2]} \right. \\ & \left. - \frac{2n_0 \hbar \Gamma_{10}^{1/2} \Phi_{10}(k_0)(\varepsilon_0 - \varepsilon_{10})}{\sqrt{m_e^*} [(\varepsilon_0 - \varepsilon_{10})^2 + (\Gamma_{10}/2)^2]} \right], \quad (30) \end{aligned}$$

where D_{cv} is the interband matrix element of dipole moment, $k_0 = \sqrt{(\hbar\omega_0 - \varepsilon_g)m_e^*}/\hbar$ is the electron wave vector corresponding to the direct interband electron transition, $\varepsilon_0 = \hbar^2 k_0^2 / 2m_e^*$ is the electron energy corresponding to this wave vector, and $\Phi_{10}(k) = \int d^2\mathbf{r} \psi_{10}(r) e^{i\mathbf{k}\mathbf{r}}$ is the Fourier transform of the ground bound state wave function. The first term in the square brackets of Eq. (30) arises from the direct optical transition. Correspondingly, the intensity of direct absorption of the probing field is $I_0 = \omega_0 m_e^* |D_{cv}|^2 E_0^2 / 2\hbar^2$. The second term there arises from the optical absorption through the bound state with the energy ε_{10} , whereas the third term originates from the quantum interference of these two absorption ways. Since the interference term changes its sign at the energy $\varepsilon_0 = \varepsilon_{10}$, we arrive at the asymmetrical structure of the absorption spectrum plotted in Fig. 5, which is typical for the Fano resonances⁴⁸ and can be easily detected experimentally.

IV. CONCLUSION

We demonstrated theoretically that a circularly polarized irradiation of graphene induces a local minimum of a repulsive potential, which results in bound electron states localized near the minimum. It is shown that the observability conditions for these states in graphene can be realized substantially easier than in usual 2D systems with

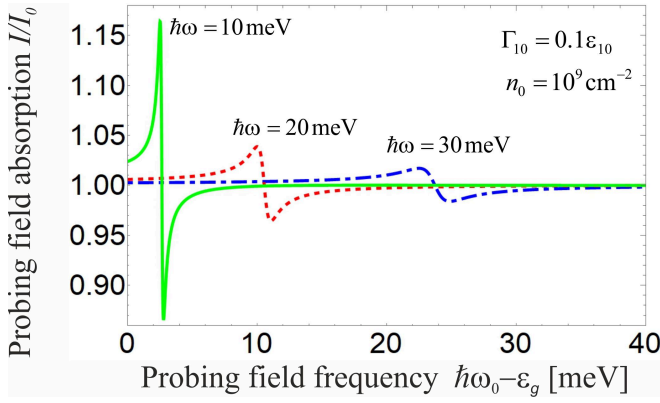


FIG. 5: The intensity of the probing field absorption, I , as a function of the probing field frequency, ω_0 , for the density of scatterers $n_0 = 10^9 \text{ cm}^{-2}$, the energy broadening $\Gamma_{10} = 0.1\epsilon_{10}$, and different frequencies of the dressing field, ω .

the parabolic electron dispersion. The states can manifest themselves, particularly, in the Breit-Wigner reso-

nant scattering of conduction electrons through them, the Kondo effect arisen from electrons localized at the states, and the asymmetrical structure of optical spectra originated from the Fano resonance of light absorption. Since these phenomena can be observed in graphene for experimentally achievable field parameters, the field-induced electron states bound by repulsive potentials can be detected in state-of-the-art measurements.

Acknowledgments

The reported study was funded by the Russian Science Foundation (project 20-12-00001).

Data availability statement

All data that support the findings of this study are included within the article (and any supplementary files).

-
- * Electronic address: oleg.kibis(c)nstu.ru
- ¹ Oka T and Kitamura S 2019 Floquet Engineering of Quantum Materials *Annu. Rev. Condens. Matter. Phys.* **10** 387
 - ² Basov D N, Averitt R D and Hsieh D 2017 Towards properties on demand in quantum materials *Nat. Mater.* **16** 1077
 - ³ Goldman N and Dalibard J 2014 Periodically driven quantum systems: effective hamiltonians and engineered gauge fields *Phys. Rev. X* **4** 031027
 - ⁴ Bukov M, D'Alessio L and Polkovnikov A 2015 Universal high-frequency behavior of periodically driven systems: from dynamical stabilization to Floquet engineering *Adv. Phys.* **64** 139
 - ⁵ Eckardt A and Anisimovas E 2015 High-frequency approximation for periodically driven quantum systems from a Floquet-space perspective *New J. Phys.* **17** 093039
 - ⁶ Casas F, Oteo J A and Ros J 2001 Floquet theory: exponential perturbative treatment *J. Phys. A* **34** 3379
 - ⁷ Kobayashi Y, Heide C, Johnson A C, Tiwari V, Liu F, Reis D A, Heinz T F and Ghimire S 2023 Floquet engineering of strongly driven excitons in monolayer tungsten disulfide *Nat. Phys.* **19** 171
 - ⁸ Nuske M, Broers L, Schulte B, Jotzu G, Sato S A, Cavalleri A, Rubio A, McIver J W and Mathey L 2020 Floquet dynamics in light-driven solids *Phys. Rev. Research* **2** 043408
 - ⁹ Liu X, Tan S, Wang Q, Zhou L and Gong J 2022 Floquet band engineering with Bloch oscillations *Phys. Rev. B* **106** 224309
 - ¹⁰ Seshadri R and Sen D 2022 Engineering Floquet topological phases using elliptically polarized light *Phys. Rev. B* **106** 245401
 - ¹¹ Koshelev K, Kachorovskii V Y and Titov M 2015 Resonant inverse Faraday effect in nanorings *Phys. Rev. B* **92** 235426
 - ¹² Kozin V K, Iorsh I V, Kibis O V and Shelykh I A 2018 Quantum ring with the Rashba spin-orbit interaction in the regime of strong light-matter coupling *Phys. Rev. B* **97** 155434
 - ¹³ Lindner N H, Refael G and Galitski V 2011 Floquet topological insulator in semiconductor quantum wells *Nat. Phys.* **7** 490
 - ¹⁴ Rechtsman M C, Zeuner J M, Plotnik Y, Lumer Y, Podolsky D, Dreisow F, Nolte S, Segev M and Szameit A 2013 Photonic Floquet topological insulator *Nature* **496** 196
 - ¹⁵ Wang Y H, Steinberg H, Jarillo-Herrero P and Gedik N 2013 Observation of Floquet-Bloch states on the surface of a topological insulator *Science* **342** 453
 - ¹⁶ Zhu T, Wang H and Zhang H 2023 Floquet engineering of magnetic topological insulator MnBi_2Te_4 films *Phys. Rev. B* **107** 085151
 - ¹⁷ Foa Torres L E F, Perez-Piskunow P M, Balseiro C A and Usaj G 2014 Multiterminal Conductance of a Floquet Topological Insulator *Phys. Rev. Lett.* **113** 266801
 - ¹⁸ Topp G E, Jotzu G, McIver J W, Xian L, Rubio A and Sentef M A 2019 Topological Floquet engineering of twisted bilayer graphene *Phys. Rev. Research* **1** 023031
 - ¹⁹ Rodriguez-Vega M, Vogl M and Fiete G A 2020 Floquet engineering of twisted double bilayer graphene *Phys. Rev. Research* **2** 033494
 - ²⁰ Rodriguez-Vega M, Vogl M and Fiete G A 2021 Low-frequency and Moiré-Floquet engineering: A review *Ann. Phys.* **435** 168434
 - ²¹ Champo A E and Naumis G G 2019 Metal-insulator transition in 8 - $Pmmn$ borophene under normal incidence of electromagnetic radiation *Phys. Rev. B* **99** 035415
 - ²² Ibarra-Sierra V G, Sandoval-Santana J C, Kunold A and Naumis G G 2019 Dynamical band gap tuning in anisotropic tilted Dirac semimetals by intense elliptically polarized normal illumination and its application to 8 - $Pmmn$ borophene *Phys. Rev. B* **100** 125302
 - ²³ Iurov A, Zhemchuzhna L, Gumbs G, Huang D, Tse W-K, Blaise K and Ejiogu C 2022 Floquet engineering of tilted and gapped Dirac bandstructure in $1T'$ - MoS_2 *Sci. Rep.* **12**

- 21348
- ²⁴ Oka T and Aoki H 2009 Photovoltaic Hall effect in graphene *Phys. Rev. B* **79** 081406(R)
 - ²⁵ Kibis O V 2010 Metal-insulator transition in graphene induced by circularly polarized photons *Phys. Rev. B* **81** 165433
 - ²⁶ Kristinson K, Kibis O V, Morina S and Shelykh I A 2016 Control of electronic transport in graphene by electromagnetic dressing *Sci. Rep.* **6** 20082
 - ²⁷ Syzranov S V, Rodionov Ya I, Kugel K I and Nori F 2013 Strongly anisotropic Dirac quasiparticles in irradiated graphene *Phys. Rev. B* **88** 241112(R)
 - ²⁸ Usaj G, Perez-Piskunow P M, Foa Torres L E F and Balseiro C A 2014 Irradiated graphene as a tunable Floquet topological insulator *Phys. Rev. B* **90** 115423
 - ²⁹ Perez-Piskunow P M, Usaj G, Balseiro C A and Foa Torres L E F 2014 Floquet chiral edge states in graphene *Phys. Rev. B* **89** 121401(R)
 - ³⁰ McIver J W, Schulte B, Stein F U, Matsuyama T, Jotzu G, Meier G and Cavalleri A 2020 Light-induced anomalous Hall effect in graphene *Nat. Phys.* **16** 38
 - ³¹ Iurov A, Zhemchuzhna L, Gumbs G, Huang D H and Fekete P 2022 Optically modulated tunneling current of dressed electrons in graphene and a dice lattice *Phys. Rev. B* **105** 115309
 - ³² Sie E J, McIver J W, Lee Y-H, Fu L, Kong J and Gedik N 2015 Valley-selective optical Stark effect in monolayer WS₂ *Nat. Mater.* **14** 290
 - ³³ Iurov A, Gumbs G and Huang D H 2019 Peculiar electronic states, symmetries, and Berry phases in irradiated alpha-T(3)materials *Phys. Rev. B* **99** 205135
 - ³⁴ Iurov A, Zhemchuzhna L, Dahal D, Gumbs G and Huang D 2020 Quantum-statistical theory for laser-tuned transport and optical conductivities of dressed electrons in alpha-T(3)materials *Phys. Rev. B* **101** 035129
 - ³⁵ Kibis O V 2019 Electron pairing in nanostructures driven by an oscillating field *Phys. Rev. B* **99** 235416
 - ³⁶ Kibis O V, Boev M V and Kovalev V M 2020 Light-induced bound electron states in two-dimensional systems: Contribution to electron transport *Phys. Rev. B* **102** 075412
 - ³⁷ Kibis O V, Kolodny S A and Iorsh I V 2021 Fano resonances in optical spectra of semiconductor quantum wells dressed by circularly polarized light *Opt. Lett.* **46** 50
 - ³⁸ Iorsh I V and Kibis O V 2021 Optically induced Kondo effect in semiconductor quantum wells *J. Phys.: Condens. Matter* **33** 495302
 - ³⁹ Kramers H A 1952 *Collected Scientific Papers* (Amsterdam: North-Holland)
 - ⁴⁰ Henneberger W C 1968 Perturbation method for atoms in intense light beams *Phys. Rev. Lett.* **21** 838
 - ⁴¹ Kondo J 1964 Resistance Minimum in Dilute Magnetic Alloys *Progress of Theoretical Physics* **32** 37
 - ⁴² de Haas W J, de Boer J, van den Berg G J 1934 The electrical resistance of gold, copper and lead at low temperatures 1934 *Physica* **1** 1115
 - ⁴³ Wilson K G 1973 The renormalization group: Critical phenomena and the Kondo problem *Rev. Mod. Phys.* **47** 773
 - ⁴⁴ Fateev V A and Wiegmann P B 1981 The exact solution of the s-d exchange model with arbitrary impurity spin S (Kondo problem) *Phys. Lett. A* **81** 179
 - ⁴⁵ Andrei N, Furuya K and Lowenstein J. H 1983 Solution of the Kondo problem *Rev. Mod. Phys.* **55** 331
 - ⁴⁶ Anderson P W 1961 Localized Magnetic States in Metals *Phys. Rev.* **124** 41
 - ⁴⁷ Coleman P 2015 *Introduction to many-body physics* (Cambridge University Press)
 - ⁴⁸ Fano U 1961 Effects of configuration interaction on intensities and phase shifts *Phys. Rev.* **124** 1866